

Studies on the Effect of a Newly Synthesized Schiff Base Compound on the Corrosion of Copper in 3% NaCl Solution

Yang Zhou, Shengtao Zhang^{*}, Lei Guo, Shenying Xu, Hao Lu, Fang Gao

School of Chemistry and Chemical Engineering, Chongqing University, Chongqing 400044, China

^{*}E-mail: stzhcq@163.com

Received: 1 December 2014 / Accepted: 31 December 2014 / Published: 19 January 2015

A new Schiff base derivative, *N,N*-dimethyl-4-((*E*)-4-((*E*)-(4-methoxybenzylidene) amino) styryl) aniline (DSA), was used as an inhibitor for copper corrosion in 3% NaCl solution. Its inhibiting performance was evaluated by a series of techniques including weight loss, electrochemical measurements, scanning electronic microscope (SEM), and theoretical calculations. Results show that the high inhibition efficiency for copper corrosion was successfully achieved just with a small amount of DSA. The DSA adsorption on copper surface obeys Langmuir adsorption isotherm. Furthermore, theoretical calculations give insightful explanations of the mechanism of DSA inhibition.

Keywords: EIS, Polarization, Weight loss, Copper, Adsorption, Theoretical calculations

1. INTRODUCTION

Copper has been one of the most important materials in industry owing to its high electrical and thermal conductivities, mechanical workability, and its relatively noble properties. It is widely used in condenser pipes of ships, coastal power plant heat exchangers, and so on. Although its resistance is quite good in nearly neutral or slightly alkaline aqueous environment, copper is still vulnerable to corrosion in harsh condition [1].

Inhibition methods are important means for the protection of metal against corrosion, especially through the organic inhibitors [2]. Recently, the inhibition of copper corrosion in NaCl solutions by different types of organic inhibitors has been extensively studied [3-5]. It is generally accepted that inhibitors act *via* their functional groups adsorbing on the metal surface, changing the corrosion resistance properties of the metal [6, 7]. Studies reported that the inhibiting effect mainly depends on some physicochemical and electronic properties of the organic compound molecule related to its functional groups, steric effects, and the π orbital character of donating electrons [8]. Among them,

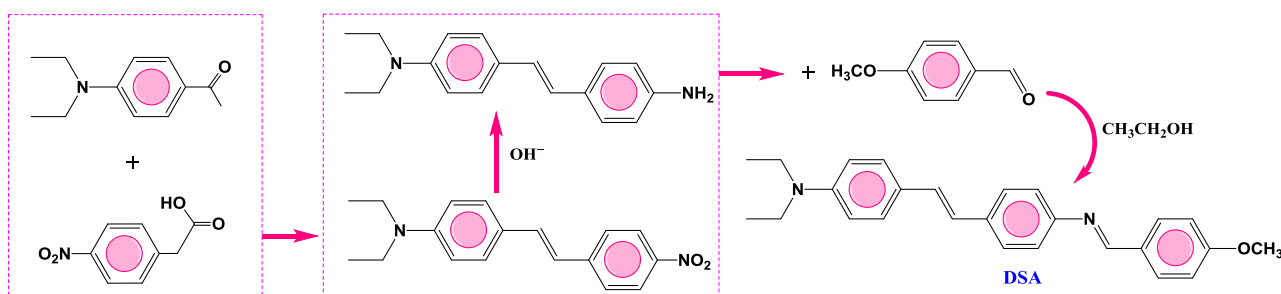
Schiff base derivatives have proved to be effective inhibitors for copper [9-11]. Based on the above considerations, DSA was synthesized as a potential inhibitor. It is expected to get adsorbed through the lone pairs of electrons on nitrogen and oxygen atoms of $-C=N-$ group and $-OCH_3$ group, as well as delocalized π -electron density on the phenyl rings by their coordination with copper surface. Further, literature survey reveals that DSA has not been reported as a corrosion inhibitor.

Thus, the aim of this work is to study the inhibiting effect of DSA on copper in 3% NaCl solution. Electrochemical polarisation, weight loss and impedance measurements are used. Meanwhile, theoretical calculations have also been used to give further insights into the adsorption and inhibiting mechanism of DSA on copper surface. The mechanisms of adsorption and inhibition are explained at the end of this paper.

2. EXPERIMENTAL

2.1. Materials and sample preparation

DSA was synthesized in our laboratory. The compound's synthetic route and molecular structure were illustrated in Scheme 1. It was purified and was characterized by 1H -NMR, ^{13}C -NMR and IR. Tetramethylsilane (TMS) was used as internal standard to determine NMR spectroscopy with Bruker 500 MHz apparatus at the room temperature. For DSA, 1H -NMR ($CDCl_3$, 500 MHz), δ (ppm): 1.097-1.125 (t, 6H, CH_3), 3.340-3.376 (m, 4H, CH_2), 3.850 (s, 3H, OCH_3), 6.660-6.678 (d, 2H, CH), 6.938-6.971 (d, 1H, ArH), 7.075-7.092 (d, 2H, ArH), 7.122 (s, 1H, ArH), 7.239-7.265 (d, 2H, ArH), 7.399-7.416 (d, 2H, ArH), 7.547-7.563 (d, 2H, ArH), 7.891-7.908 (d, 2H, ArH), 8.599 (s, 1H, NCH); ^{13}C -NMR ($CDCl_3$, 125 MHz), δ (ppm): 162.295, 159.360, 159.306, 150.370, 130.746, 129.544, 128.638, 127.911, 127.152, 127.083, 123.583, 121.901, 114.732, 112.708, 55.837, 44.157, 12.901; IR (KBr) ν : 2930, 1681, 1603, 1520, 1355, 1163, 966, 836 cm^{-1} .



Scheme 1. The synthetic route of and molecular structure of newly synthesized DSA.

DSA was dissolved in 3% NaCl at different concentrations, from 0.04 to 0.10 $mmol L^{-1}$ (mM, for short). The solution in the absence of DSA was used as a blank for comparison. Tests were performed on pure copper ($Cu > 97.5\%$). In the weight loss experiments, copper samples were mechanically cut into 2.00 cm \times 2.00 cm \times 1.00 cm dimensions. While in the electrochemical

experiments, they were cut into 1.00 cm × 1.00 cm × 1.00 cm cubes. The cube was embedded in epoxy resin in such a way that the flat surface was in contact with the aggressive solution (test solution) and with 1 cm² exposed area. Before each test, all of the specimens were mechanically abraded with emery paper up to 2000 grit, then rinsed with distilled water, degreased ultrasonically in acetone and dried at room temperature.

During the weight loss and electrochemical measurements, the temperature of solution was controlled at 303 K by a water thermostat with an accuracy of 1 K, and all experiments were open to the air and carried out under static conditions.

2.2. Electrochemical tests

The electrochemical experiments were performed in a classical three-electrode cell assembly with copper specimen as the working electrode, platinum foil of 1.5 cm × 1.5 cm as the counter electrode, and a saturated calomel electrode (SCE) provided with a Luggin capillary as the reference electrode. All potentials were referred to SCE reference electrode. Electrochemical impedance spectroscopy (EIS) measurements were carried out at the open circuit potential (E_{OCP}). The ac frequency range extended from 100 kHz to 10 mHz with a 10 mV peak-to-peak sine wave as the excitation signal. Then the impedance data were analyzed and fitted. The polarization curves were obtained from -250 to +250 mV (vs. E_{OCP}) with 0.5 mV s⁻¹ scan rate, and the data were collected and analyzed.

2.3. Weight loss experiments

Copper specimens in triplicate were immersed in the test 3% NaCl solution for 9 days under different conditions. After that, the specimens were removed from the solutions, rinsed in water and absolute ethanol, finally dried and weighted. Weight loss experiments were utilized to calculate the mean corrosion rate.

2.4. SEM analysis

The surface morphology of specimens after immersion in 3% NaCl in the absence and presence of different concentration of DSA was performed on a KYKY2800B SEM. The accelerating voltage was 25 kV.

2.5. Calculation methods

The molecular dynamics (MD) simulations were performed using the software, Material Studio 6.0, Forcite module. Cu(111) surface was chosen for the simulation study. COMPASS [12] (Condensed Phase Optimized Molecular Potentials for Atomistic Simulation Studies) force field was used to optimize the structures of all components of the system of interest represents a technology

break-through in force field method. The MD simulation of the interaction between involved molecules and the Cu(111) surface was carried out in a simulation box ($28.1 \text{ \AA} \times 25.5 \text{ \AA} \times 57.8 \text{ \AA}$) with periodic boundary conditions to model a representative part of the interface devoid of any arbitrary boundary effects. The Cu(111) plane was first cleaved from copper crystal, and then the surface was optimized to the energy minimum. The DSA molecule was firstly optimized to most stable configuration with molecular mechanics method. The amorphous cell was then constructed with the optimized inhibitor and 800 water molecules using Amorphous Cell module. The configurations of (DSA + 800 H₂O) interacting with Cu(111) are obtained by “build Layers” tool. The MD simulation was performed under 303 K, NVT ensemble, with a time step of 1 fs and simulation time of 1 ns.

Quantum chemical calculations were conducted with the DMol³ module [13]. All electronic calculations of DSA molecule were accomplished by GGA/BLYP method with a double numerical with *d* and *p* polarization (DNP) basis set [14]. The computationally economical DNP basis set is comparable in size to the Gaussian-type 6-31G (*d*, *p*) basis set and the reliability of this level of theory in studying the organic molecule has been confirmed [15, 16]. The convergence tolerance for geometry optimization was 2.7×10^{-4} eV for energy, 0.054 eV/Å for force, and 0.005 Å for displacement, respectively. The orbital cut off was set to 3.7 Å, and frequency analysis was performed to ensure the calculated structure being the minimum point on potential energy surface (without imaginary frequency).

3. RESULTS AND DISCUSSION

3.1. Potentiodynamic polarization

Figure 1 represents the potentiodynamic polarization curves of copper in 3% NaCl in the presence and absence of various concentrations of DSA.

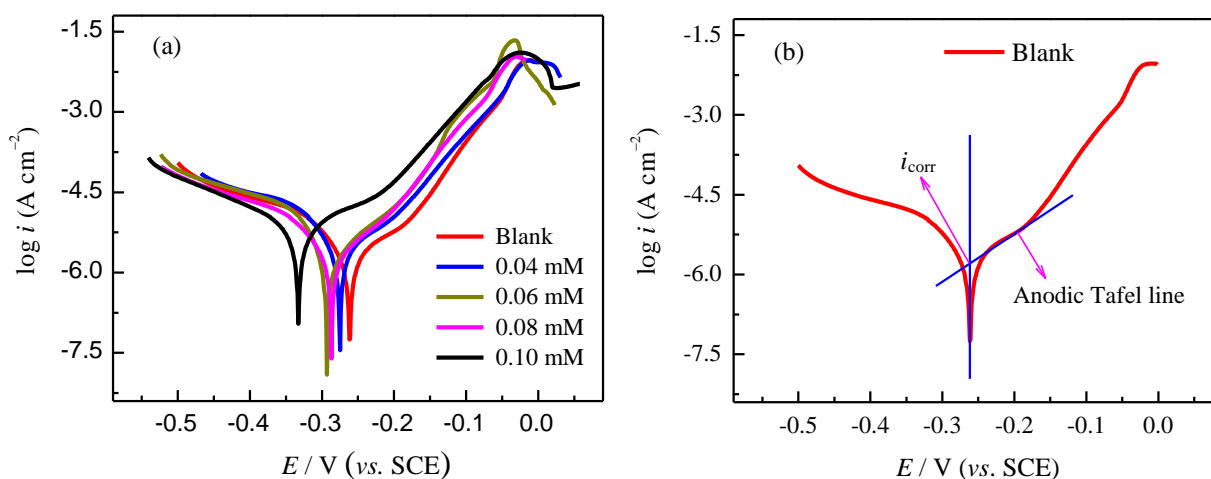


Figure 1. (a) Potentiodynamic polarization curves for copper in 3% NaCl in the presence of different concentrations of DSA; (b) Tafel extrapolation of the anodic polarization curve.

Table 1. Parameters for copper in 3% NaCl solution with different concentrations of DSA.

C (mM)	I_{corr} ($\mu\text{A cm}^{-2}$)	E_{corr} (V)	β_a (mV dec^{-1})	IE%
Blank	13.46	-0.334	225	/
0.04	2.249	-0.242	98	83.29
0.06	1.945	-0.274	107	85.55
0.08	1.731	-0.286	105	87.14
0.10	1.412	-0.294	95	89.51

From Fig. 1a, it can be clearly seen that DSA has significantly decreased the corrosion rate, shifting polarization curves to lower values of corrosion current densities. This result indicates that the addition of inhibitor reduces copper anodic dissolution and also retards the oxygen reduction. This inhibition became more pronounced with increasing DSA concentration.

It has been known that in the Tafel extrapolation method, the use of both the anodic and cathodic Tafel regions is undoubtedly preferred over the use of only one Tafel region [17]. However, because the transfer of oxygen from the bulk solution to the copper/solution interface will strongly affect the rate of oxygen reduction, the cathodic polarization curves deviate from the Tafel behaviour, exhibiting a limiting diffusion current. Therefore, the corrosion current densities were obtained by extrapolation of the anodic polarization curves to E_{corr} alone in this study, as shown in Fig. 1b. The kinetics of electron transfer at the metal/solution interface can be shown using the Butler–Volmer equation [18]. Moreover, for the copper electrode in 3% NaCl solution the Butler–Volmer equation is modified to give:

$$i = i_{\text{corr}} \left[e^{n\alpha F(E-E_{\text{corr}})/RT} - e^{-(1-\alpha)nF(E-E_{\text{corr}})/RT} \right] \quad (1)$$

where i_{corr} is the corrosion current density at the corrosion potential E_{corr} , α is the transfer coefficient (usually 0.5), and n is the number of electrons transferred. When the rate of the back reaction is negligible, Eq. (1) gives:

$$E = a + b \log i \quad (2)$$

where a and b are constants. In Eq. (2), when $E = E_{\text{corr}}$, then $i = i_{\text{corr}}$. This is the basis for the Tafel extrapolation.

Associated electrochemical parameters such as corrosion potential (E_{corr}), anodic Tafel slope (β_a), and corrosion current density (i_{corr}) are summarized in Table 1. The inhibition efficiency (IE%) was evaluated using the following equation:

$$IE\% = \frac{i_{\text{corr}}^0 - i_{\text{corr}}}{i_{\text{corr}}^0} \times 100 \quad (3)$$

where i_{corr}^0 and i_{corr} are the corrosion current densities in the absence and the presence of inhibitor, respectively.

As shown in Table 1, the values of i_{corr} decrease gradually with increasing DSA concentration, and the inhibition efficiency reaches a maximum value of 89.51% at 0.10 mM. This indicates that DSA shows good inhibition effect on copper in 3% NaCl solution. The significant improvement of the corrosion protection may originate from the adsorption of DSA on copper surface and the hydrophobic nature of the phenyl groups of DSA.

3.2. Electrochemical impedance spectroscopy (EIS)

To get further information concerning the inhibition process, EIS measurements on the copper electrode were performed. Fig. 2 shows the Nyquist plots in the presence and absence of DSA, respectively. Several convex arcs exist and each diameter of the arcs increases with the inhibitor concentration increases. When the concentration of DSA was 0.10 mM, the capacitive reactance arc radius was the greatest.

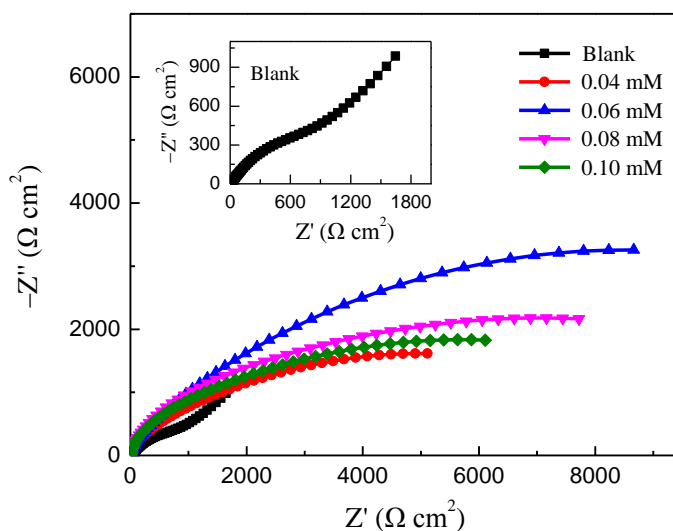


Figure 2. Nyquist diagrams for copper electrode in 3% NaCl solution with and without DSA.

The equivalent circuit model employed for this system is shown in Fig. 3. As it is seen from the Fig. 2, the Nyquist plot obtained in blank solution contains a capacitive loop in high frequency region followed by a straight line in low frequencies. The low frequency is generally called as Warburg's impedance [19]. The high frequency capacitive loop is related to the charge transfer resistance. The low frequency straight line implies that the corrosion of copper in 3% NaCl solution is diffusion controlled which may be due to either the transportation of corrosive ions and soluble corrosion products at the metal/solution interface or the diffusion of dissolved oxygen to the copper surface [20]. For the copper electrodes in NaCl solution with DSA inhibitor, the Warburg impedance disappears at low frequencies, only some large capacitive loops are observed in Nyquist plots. The disappearance of Warburg impedance indicates that the DSA is sufficiently densely packed to prevent the diffusion process of corrosion reaction and the copper corrosion is controlled by the charge transfer process. The diameters of the capacitive loops increase with increasing DSA concentration, suggesting that the inhibitor absorbed on the copper surface increases corrosion resistance and reduces the corrosion rate. Therefore, two equivalent circuit models are proposed in order to fit and analyze the EIS data. Model a (Fig. 3a) involving Warburg impedance is used to simulate corrosion reaction on the bare copper, while model b (Fig. 3b) is for the copper with inhibitors, which has been widely used to estimate the barrier and protection properties of corrosion inhibitors [21-23]. The corresponding fitting results are listed in Table 2.

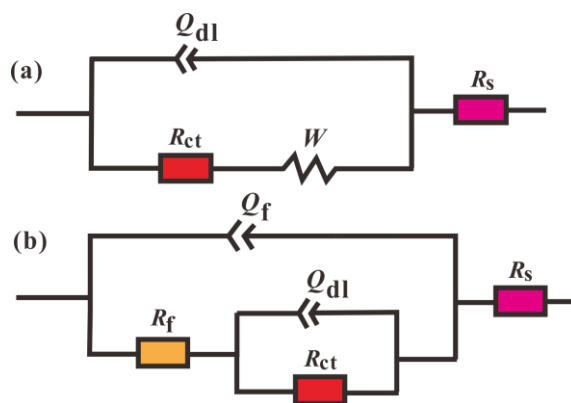


Figure 3. The equivalent circuit model used to fit the EIS experiment data.

In Fig. 3, R_s shows the the solution resistance, R_{ct} reflects the charge-transfer resistance, R_f is the resistance of the film formed on the copper surface, Q_{dl} and Q_f represent the constant phase elements (CPEs), and W is the Warburg impedance. The impedance of a CPE is defined as follows [24]:

$$Z_{CPE} = Y_0^{-1} (j\omega)^{-n} \tag{4}$$

where Y_0 is the modulus, ω is the angular frequency, j is the imaginary root, and n is a deviation parameter, which determines the divergence of the CPE from an ideal capacitor varying between 0 and 1. When $n = 0$, CPE represents a resistance, for $n = 1$, an ideal capacitance. The inhibition efficiency was calculated from R_{ct} according to the equation:

$$IE\% = \frac{R_{ct} - R_{ct}^0}{R_{ct}} \times 100 \tag{5}$$

where R_{ct}^0 and R_{ct} are the charge transfer resistance in the absence and presence of the inhibitor, respectively.

Table 2. Impedance parameters of copper in 3% NaCl solution with different concentrations of DSA.

C (mM)	R_s ($\Omega \text{ cm}^2$)	R_f ($\Omega \text{ cm}^2$)	R_{ct} ($\Omega \text{ cm}^2$)	Q_f $Y_0 (\times 10^{-5} \text{ S s}^n \text{ cm}^{-2})$ n_1	Q_{dl} $Y_0 (\times 10^{-5} \text{ S s}^n \text{ cm}^{-2})$ n_2	W ($\times 10^{-7} \text{ S s}^{0.5} \text{ cm}^{-2}$)	$IE\%$		
Blank	3.749	/	1037	/	/	4.703	0.588	2.54	/
0.04	1.678	3.610	8300	26.14	0.380	1.997	0.921	/	87.51
0.06	1.722	3.681	9810	18.15	0.375	1.531	0.975	/	89.43
0.08	2.207	3.800	12920	11.83	0.940	1.256	0.952	/	91.97
0.10	2.494	4.171	14500	10.11	0.943	1.117	0.923	/	92.84

On the basis of Table 2, the addition of DSA increases the R_{ct} and R_f values. It seems to be enhanced with the increasing of the inhibitor concentration. $IE\%$ values reach the maximum 92.84% at the concentration of 0.10 mM. Table 2 shows that the Q_{dl} and Q_f values decrease with increasing DSA

concentration. The film capacitance (C_f) and the electrical double layer capacitance (C_{dl}) could be expressed as follows [25, 26]:

$$C_f = \frac{F^2 S}{4RT} \quad (6)$$

$$C_{dl} = \frac{\varepsilon^0 \varepsilon}{d} S \quad (7)$$

Herein, S is the surface area of the electrode exposed to the corrosive solution, F is the Faraday's constant, ε^0 is the permittivity constant of the air, ε is the local dielectric constant of the film, and d is the thickness of the electrical double layer. The decrease of C_f can be attributed to increasing inhibitor adsorption which decreases the exposed electrode surface area. On the other hand, the decrease of C_{dl} can result from a decrease in local dielectric constant and/or an increase in the thickness of the electrical double layer.

3.3. Weight loss test and the adsorption isotherm

The corrosion rate (v) can be obtained from weight loss measurements for different concentrations of DSA in 3% NaCl, as provided in Table 3. Corrosion rate v ($\text{mg cm}^{-2} \text{h}^{-1}$) and the corrosion inhibition efficiency were obtained by the following formulas:

$$v = \frac{\Delta W}{S \cdot t} \quad (8)$$

$$IE\% = \frac{v_0 - v_i}{v_0} \times 100 \quad (9)$$

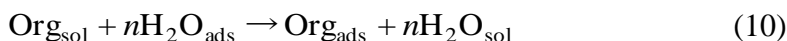
where ΔW is the average weight loss (mg), S is the surface area of specimens (cm^2), t is the immersion time (h); v_0 and v_i signified the corrosion rate in the absence and presence of inhibitors, respectively.

It can be seen that the corrosion inhibitor can protect copper perfectly and the inhibition efficiency increased with increasing concentrations. The corrosion rate reached to the minimum at 0.10 mM, but the inhibition efficiency reached to maximum. This phenomenon suggests that the DSA molecules act by adsorption on the copper surface.

Table 3. Weight loss data of copper in 3% NaCl solution with different concentrations of DSA for 9 days.

C (mM)	v ($\text{mg cm}^{-2} \text{h}^{-1}$)	θ	η (%)
Blank	9.82	/	/
0.04	1.76	0.8207	82.07
0.06	1.39	0.8584	85.84
0.08	0.98	0.9002	90.02
0.10	0.86	0.9124	91.24

The adsorption of organic inhibitor molecules from the aqueous solution can be considered as a quasi-substitution process between the organic compounds in the aqueous phase [Org_{sol}] and water molecules associated with the metallic surface [$\text{H}_2\text{O}_{\text{ads}}$] as represented by the following equilibrium [27]:



where n is the number of water molecules removed from the metal surface for each molecule of inhibitor adsorbed. The adsorption isotherm can give important information about the interaction of the DSA inhibitor and metal surface. In order to clarify the nature and the strength of adsorption, the experimental results were fitted to a series of adsorption isotherms, and the best fit was obtained with the use of the Langmuir adsorption isotherm, which is presented graphically in Fig. 4. The correlation coefficient (0.999) is close to 1 which confirms this assumption. Langmuir adsorption isotherm can be expressed by the following equation [28]:

$$\frac{C}{\theta} = \frac{1}{K_{\text{ads}}} + C \quad (11)$$

where θ is the surface coverage (see Table 3), C is inhibitor concentration, and K_{ads} is the adsorption equilibrium constant. This isotherm assumed that the adsorbed molecules occupied only one site and there was no interaction with other molecules adsorbed.

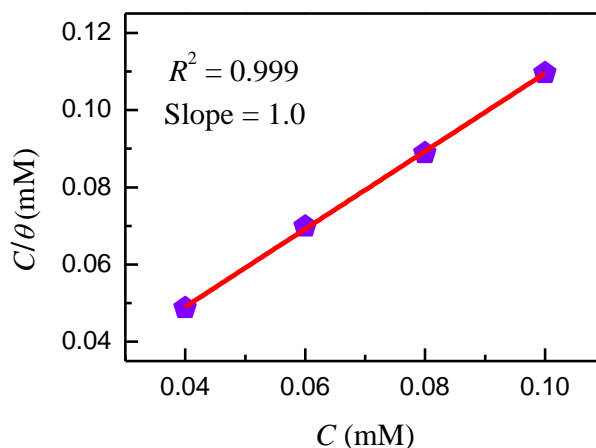


Figure 4. Langmuir adsorption isotherm of DSA on the surface of copper.

Gibbs free energy (ΔG_{ads}) could be calculated with the following equation [29]:

$$\Delta G_{\text{ads}} = -RT \ln(55.5K_{\text{ads}}) \quad (12)$$

where R ($\text{J mol}^{-1} \text{K}^{-1}$) is the gas equilibrium constant, T (K) is the temperature, 55.5 (mol L^{-1}) is the molecular concentration of water in solution. In Fig. 4, the intercept on the vertical axis is the value of $1/K_{\text{ads}}$, which is 8.73×10^{-6} . Then according to Eq. (12), we calculated the $\Delta G_{\text{ads}} = -39.4 \text{ kJ mol}^{-1}$. The negative value of ΔG_{ads} obtained herein, indicated that the adsorption process of DSA on the metal surface is a spontaneous one. Generally, if the absolute value of ΔG_{ads} is lower than 20 kJ mol^{-1} , the type of adsorption is regarded as physisorption, and the corrosion inhibition takes action due to the electrostatic interactions between the charged molecules and the charged metal. If the absolute

value of ΔG_{ads} is higher than 40 kJ mol^{-1} , it functions by chemisorption due to the covalent bond formed by the charge sharing or a charge transfer from (to) the inhibitor molecule to (from) the metal surface [30]. According the obtained value of ΔG_{ads} ($-39.4 \text{ kJ mol}^{-1}$), it can be suggested that the adsorption of DSA involves two types of interaction, chemisorption and physisorption.

3.4. SEM Analysis

The SEM images of copper specimens exposed to 3% NaCl solutions for 3 days with and without DSA are given in Fig. 5. Before corrosion, the surface morphology of the sample was a freshly polished copper surface, as seen in Fig. 5a. After corrosion in 3% NaCl solution, the surface morphology becomes porous and rough as shown in Fig. 5b, which means the copper, was severely corroded. Fig. 5c~d show the morphological features of the inhibited surface. Compared with the blank, corrosion degree decreased obviously in the presence of the inhibitor. Especially when the concentration is 0.10 mM, the surface is very smooth. The inhibitor may form a protective film adsorbed on the copper surface, resulting in a decrease in the contact between copper and the aggressive solution.

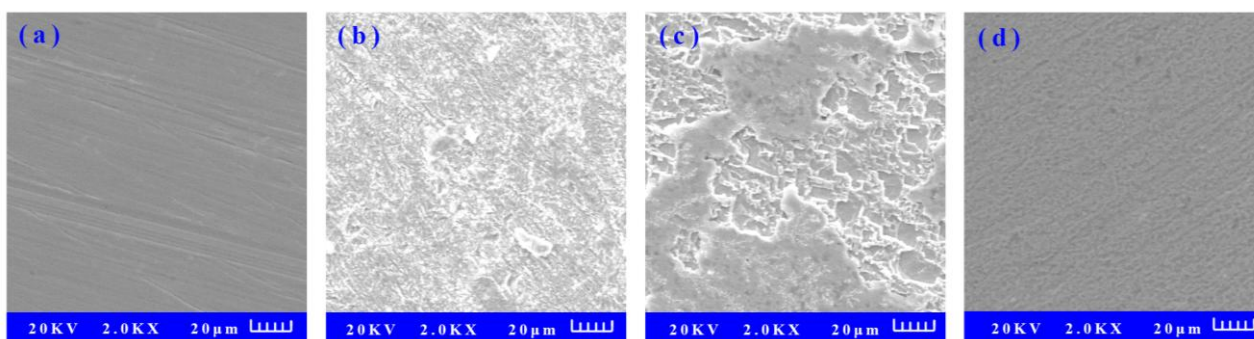


Figure 5. SEM micrographs of freshly polished copper specimen (a), the specimen immersed in 3% NaCl solutions for 3 days without (b), and with 0.06 mM (c), 0.10 mM (d) DSA.

3.5. Quantum chemical calculations

To investigate the relationship between the molecular structure of this compound and its inhibition effect, quantum chemical calculations were performed. The frontier molecular orbital energies (E_{HOMO} and E_{LUMO}) are significant parameters for the prediction of the reactivity of a chemical species [31]. The frontier molecular orbital density distribution, the total electron density, as well as the electrostatic potential (ESP) of DSA molecule are shown in Fig. 6. Apparently, both the HOMO and LUMO orbitals are of π -type and are spread through the whole molecule. Thus, all the benzene rings are susceptible sites for electrophilic attacks. From an overall perspective, DSA is a strong electron donor, for which evidence can be found in the total electron density (Fig. 6c). This has been also confirmed by the electrostatic potential map (Fig. 6d), in which the negatively charged red

regions are located at the upper/lower surface of the molecular skeleton. These electron-rich areas would be preferred sites for adsorption to metal surfaces.

Employing the finite difference approximation, the ionization potential (I) and electron affinity (A) of the inhibitors are calculated using the equations [32]:

$$I = E_{(N-1)} - E_N \quad (13)$$

$$A = E_N - E_{(N+1)} \quad (14)$$

where $E_{(N-1)}$, E_N , and $E_{(N+1)}$ are the ground state energies of the system with $N-1$, N , and $N+1$ electrons, respectively. The values of ionization potential (I) and electron affinity (A) were considered for the calculation of the electronegativity (χ) and global hardness (η): $\chi = (I + A)/2$, $\eta = (I - A)/2$. The fraction of electrons transferred from (to) the inhibitor molecules to (from) the metal surface (ΔN) was calculated according to Pearson theory as follows [33]:

$$\Delta N = \frac{\chi_{\text{metal}} - \chi_{\text{inh}}}{2(\eta_{\text{metal}} + \eta_{\text{inh}})} = \frac{\Phi - \chi_{\text{inh}}}{2\eta_{\text{inh}}} \quad (15)$$

where the work function (Φ) is used for the electronegativity of copper surface, and the global hardness is neglected by assuming that for a metallic bulk $I = A$ because they are softer than the neutral metallic atoms [34].

The computed quantum chemical properties such as E_{HOMO} , E_{LUMO} , ionization potential (I), electron affinity (A), and the fraction of transferred electrons (ΔN) are listed in the Table 4. As seen from the table, the positive ΔN value indicate that the electron transfer from the DSA molecule to copper surface is available.

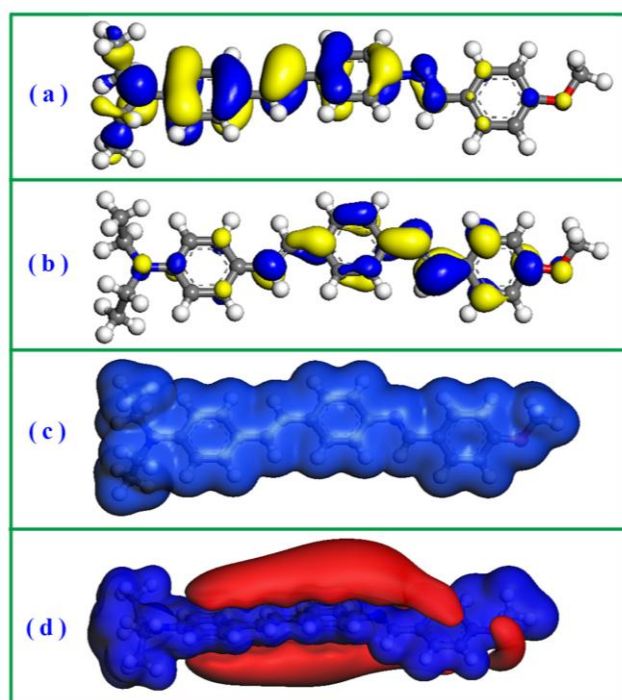


Figure 6. Electronic properties of the DSA molecule: (a) HOMO orbital, (b) LUMO orbital, (c) total electron density, and (d) electrostatic potential.

Table 4. Quantum chemical parameters derived for DSA calculated with the GGA/BLYP/DNP method.

E_{HOMO} (eV)	E_{LUMO} (eV)	ΔE (eV)	μ (Debye)	I (eV)	A (eV)	χ	η	ΔN
-4.175	-2.483	1.692	4.238	4.441	2.195	3.318	1.123	0.374

3.6. Molecular dynamics (MD) simulations

The molecular dynamics (MD) simulations have been employed to predict the adsorption of DSA molecule on Cu(111) surface. And the simulations were made with the participation of water so as to make the results more practical. Fig. 7 shows the initial and equilibrium configurations of DSA molecule adsorbed on Cu(111) surface in water solution. As time progresses, DSA molecule gradually moves to the iron surface, and when the adsorption process reaches a balance, all the atoms are almost in the same plane, and the DSA molecule plane is nearly parallel to the target surface. Actually, we have predicted this configuration in the quantum chemical analysis mentioned above. The DSA molecule is subjected to a substantial degree of deformation. Generally, the deformation degree of absorbed molecule can be evaluated by deformation energy (E_{deform}):

$$E_{\text{deform}} = E_{\text{bonded}} - E_{\text{free}} \quad (16)$$

where E_{bonded} and E_{free} are the energies of a single inhibitor molecule in the adsorbed and free states, respectively. As Table 5 shows, the E_{deform} of DSA is greater than 100 kJ mol^{-1} , indicating that this molecule have deformed obviously.

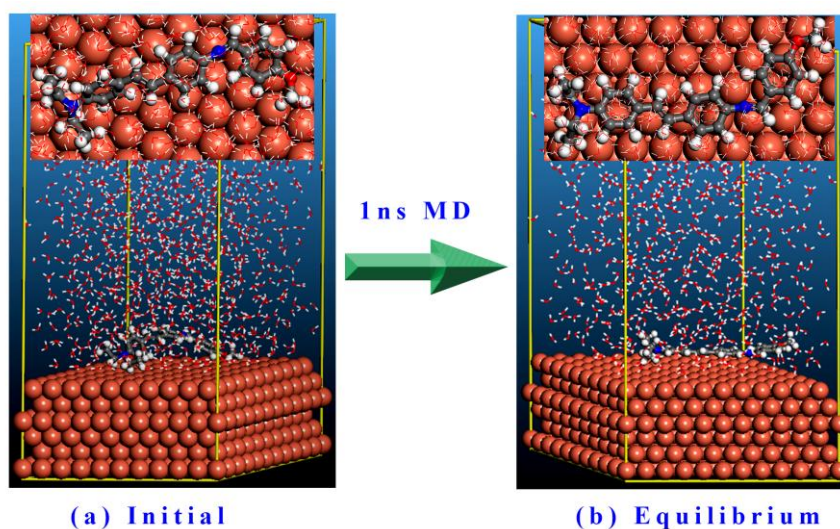


Figure 7. Configurations of DSA molecule adsorbed on Cu(111) surface in water solution: (a) initial and (b) equilibrium. (Inset images show the on-top views)

Quantitative appraisal of the interaction was achieved by calculating the adsorption energy (E_{ads}) using Eq. (16):

$$E_{\text{ads}} = E_{\text{complex}} - (E_{\text{Cu}} + E_{\text{inh}}) \quad (17)$$

where E_{complex} is the total energy of the surface and inhibitor, E_{Cu} and E_{inh} is the total energy of the copper surface and free inhibitor molecule, respectively. The binding energy is defined to be the opposite of the interaction energy, *i.e.*, $E_{\text{binding}} = -E_{\text{ads}}$. A larger E_{binding} implies the corrosion inhibitor combines with the copper surface more easily and tightly, therefore, the inhibitive performance will be better. One of the most important quantities when considering the results in solution is the solvation energy (E_{sol}). It indicates the extent of the solute–solvent interactions on the different inhibitors (*i.e.*, it is an indication of solubility). A high tendency to be solvated implies that the inhibitor spends more time in the solvent and has fewer tendencies to interact with the metal surface [35]. In this work, E_{sol} was calculated according to the following equation:

$$E_{\text{sol}} = E_{\text{inh+water}} - (E_{\text{water}} + E_{\text{inh}}) \quad (18)$$

where $E_{\text{water+inh}}$ and E_{water} are the total potential energy of the inhibitor molecule plus the water molecules and the pure water phase, respectively. The binding energy of the interaction system and the corresponding solvation energy of DSA molecule are listed in Table 5. The binding energy in Table 5 is positive, showing that the combination processes of DSA with copper surface is exothermic. While a relatively high value of E_{sol} of DSA may originate from the large molecular volume.

Moreover, for the deeper insight of the molecule's interaction with the surrounding medium and copper surface, the energy differences (ΔE) were calculated according the below formula [36]:

$$\Delta E = E_{\text{without-inh}} - E_{\text{with-inh}} \quad (19)$$

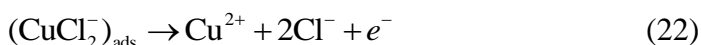
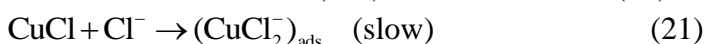
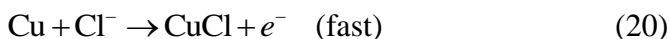
where $E_{\text{with-inh}}$ is the energy of whole system with inhibitor molecule inside, and $E_{\text{without-inh}}$ is the energy of the system in which the inhibitor molecule has been removed. The differences of non-bond energies ($\Delta E_{\text{non-bond}}$), which include van der Wals energy (ΔE_{vdw}), long range correction energy (ΔE_{lrc}) and electrostatic energy (ΔE_{elec}), were examined and given in Table 5. It is not hard to conclude that the van der Wals and electrostatic interactions are the dominant factors for the inhibitor absorption, and the contribution from the former interaction is greater than the latter.

Table 5. Several energy parameters (all in kJ mol^{-1}) for the DSA/Cu(111) system.

E_{ads}	E_{binding}	E_{deform}	E_{sol}	ΔE_{vdw}	ΔE_{elec}	ΔE_{lrc}	$\Delta E_{\text{non-bond}}$
-506.3	506.3	293.1	-106.5	493.5	122.7	4.8	621.1

3.7. Mechanism of adsorption and inhibition

A clarification of the mechanism of inhibition requires full knowledge of the interaction between the protective organic inhibitor and the metal surface. The corrosion behavior of copper in NaCl solution has received considerable attention in the literature [37, 38]. The mechanism of the anodic dissolution of copper is shown in the following equations [39]:



The anodic copper dissolution was controlled by both electrodisolution of copper and diffusion of soluble $(\text{CuCl}_2)_{\text{ads}}$ to the bulk solution. Cathodic chemical process occurs as following:



As illustrated in Fig. 8, a mechanism has been proposed to explain the high inhibiting efficiency of DSA. It attributes the phenomenon to the formation of an adsorbed layer of DSA molecules, *i.e.*,



where $\text{Cu} : \text{DSA}_{(\text{ads})}$ refers to DSA adsorbed on the copper surface. Yet, at low DSA concentrations, a localized corrosion may occur at anode area, as validated by Fig. 5c. A perfect DSA organic film can be formed on copper surface with increasing concentration of DSA, which can be seen as a barrier to copper dissolution and O_2 reduction. Several types of adsorption may take place in the inhibiting phenomena involving DSA molecules at the copper surface as follows: (i) non-covalent interaction of DSA (or protonated) molecules with copper atoms (physisorption); (ii) interaction between unshared electron pairs of N/O atoms or π -electrons of phenyl ring and copper surface (chemisorption); and (iii) a combination of the above processes.

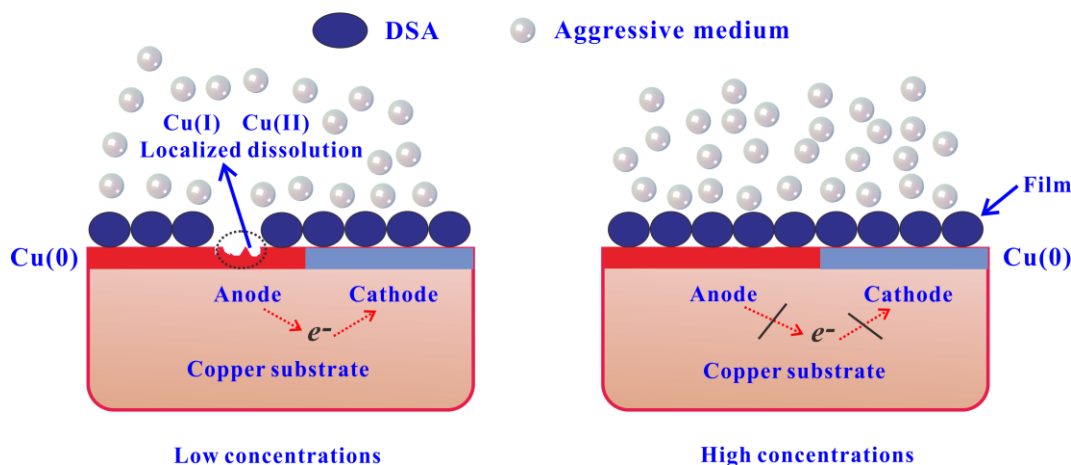


Figure 8. Proposed mechanism for the adsorption of DSA molecules on the copper surface in NaCl medium.

4. CONCLUSIONS

(1) DSA exhibited good inhibition for copper corrosion in 3% NaCl solution. The inhibition efficiency increased with increasing concentration of DSA and reached its maximal value of 92.84% at 0.10 mM.

(2) EIS plots show that the charge transfer resistance increases and double layer capacitance declines in the presence of DSA, which is caused by the adsorption of DSA molecules on the copper surface.

(3) Adsorption of the DSA on copper surface obeys the Langmuir isotherm, and the

negative values of G_{ads} show the adsorption of this compound was a spontaneous process. The adsorption of it was the result of the combined action of the physical and chemical interactions.

(4) SEM micrographs showed that the inhibitor molecules form a good protective film on the copper surface.

(5) MD simulations reveal that DSA molecules adsorb on the copper surface in a nearly flat manner.

ACKNOWLEDGEMENTS

This work was supported by Natural Science Foundation of China (No. 21376282), and Chongqing Innovation Fund for Graduate Students (No. CYB14019).

References

1. G. Kear, B.D. Barker, F.C. Walsh, *Corros. Sci.* 46 (2004) 109.
2. B.E.A. Rani, B.B.J. Basu, *Int. J. Corros.* 2012 (2012) 1.
3. M.M. Singh, R.B. Rastogi, B.N. Upadhyay, *Bull. Electrochem.* 12 (1996) 26.
4. G. Kilmceker, H. Demir, *Anti-Corros. Method. M.* 60 (2013) 134.
5. H. Baeza, M. Guzman, R. Lara, *Int. J. Electrochem. Sci.* 8 (2013) 7518.
6. H. Gerengi, K. Schaefer, H.I. Sahin, *J. Ind. Eng. Chem.* 18 (2012) 2204.
7. M.M. Antonijevic, M.B. Petrovic, *Int. J. Electrochem. Sci.* 3 (2008) 1.
8. S. John, A. Joseph, *Mater. Corros.* 64 (2013) 625.
9. S.M. Shaban, A. Saied, S.M. Tawfik, A. Abd-Elaal, I. Aiad, *J. Ind. Eng. Chem.* 19 (2013) 2004.
10. M. Hosseini, S.F.L. Mertens, M. Ghorbani, M.R. Arshadi, *Mater. Chem. Phys.* 78 (2003) 800.
11. H. Ma, S.H. Chen, L. Niu, S.X. Shang, S.L. Li, S.Y. Zhao, Z.L. Quan, *J. Electrochem. Soc.* 148 (2001) 208.
12. H. Sun, *J. Phys. Chem. B* 102 (1998) 7338.
13. B. Delley, *J. Chem. Phys.* 113 (2000) 7756.
14. C.T. Lee, W.T. Yang, R.G. Parr, *Phys. Rev. B* 37 (1988) 785.
15. J. Zhang, G. Qiao, S. Hu, Y. Yan, Z. Ren, L. Yu, *Corros. Sci.* 53 (2011) 147.
16. E.E. Oguzie, Y. Li, S.G. Wang, F. Wang, *RSC Adv.* 1 (2011) 866.
17. E. McCafferty, *Corros. Sci.* 47 (2005) 3202.
18. J.M. Saveant, D. Tessier, *J. Electroanal. Chem.* 65 (1975) 57.
19. D.D. Macdonald, *Electrochim. Acta* 51 (2006) 1376.
20. G. Quartarone, M. Battilana, L. Bonaldo, T. Tortato, *Corros. Sci.* 50 (2008) 3467.
21. D. Wang, B. Xiang, Y. Liang, S. Song, C. Liu, *Corros. Sci.* 85 (2014) 77.
22. S. Hong, W. Chen, Y. Zhang, H.Q. Luo, M. Li, N.B. Li, *Corros. Sci.* 66 (2013) 308.
23. A.O. Yuce, G. Kardas, *Corros. Sci.* 58 (2012) 86.
24. G.J. Brug, A.L.G. Vandeneeden, M. Sluytersrehabach, J.H. Sluyters, *J. Electroanal. Chem.* 176 (1984) 275.
25. P. Simon, Y. Gogotsi, *Nat. Mater.* 7 (2008) 845.
26. S. John, A. Joseph, *Ind. Eng. Chem, Res.* 51 (2012) 16633.
27. I. Ahamad, M.A. Quraishi, *Corros. Sci.* 51 (2009) 2006.
28. K.Y. Foo, B.H. Hameed, *Chem. Eng. J.* 156 (2010) 2.
29. Y. Marcus, *J. Chem. Soc., Faraday Trans.* 87 (1991) 2995.
30. F.M. Donahue, K. Nobe, *J. Electrochem. Soc.* 112 (1965) 886.
31. I. Lukovits, E. Kalman, F. Zucchi, *Corrosion* 57 (2001) 3.
32. S.B. Liu, *Acta Phys. Chim. Sin.* 25 (2009) 590.

33. R.G. Pearson, *Inorg. Chem.* 27 (1988) 734.
34. L. Guo, W.P. Dong, S.T. Zhang, *RSC Adv.* 4 (2014) 41956.
35. E.E. Ebenso, M.M. Kabanda, L.C. Murulana, A.K. Singh, S.K. Shukla, *Ind. Eng. Chem, Res.* 51 (2012) 12940.
36. J.P. Zeng, J.Y. Zhang, X.D. Gong, *Comput. Theor. Chem.* 963 (2011) 110.
37. F. Arjmand, A. Adriaens, *Materials* 5 (2012) 2439.
38. Y. Zhao, C.J. Lin, Y. Li, R.G. Du, J.R. Wang, *Acta Phys. Chim. Sin.* 23 (2007) 1342.
39. K.F. Khaled, *Appl. Surf. Sci.* 255 (2008) 1811.

© 2015 The Authors. Published by ESG (www.electrochemsci.org). This article is an open access article distributed under the terms and conditions of the Creative Commons Attribution license (<http://creativecommons.org/licenses/by/4.0/>).